

Fast-Charge Limitations for Graphite Anodes with Si as Capacity-Enhancing Additive

Fabian Jeschull^[a] and Sigit Trabesinger^{*[a]}

Rate capability is always coming into the question when new materials are characterized; however, this question also arises when blends of different electroactive materials are used. This study was dedicated to the charge capabilities of graphite-Si blends, in which Si acts as a capacity-enhancing electrode additive (≤ 20 wt.% Si). As delithiated Si is considered poorly electronic conductor, one would assume that the presence of Si induces additional internal resistance that hampers fast charging of this type of electrodes. Current-interruption measurements demonstrate that the internal resistance of graphite-Si

blends increases proportionally to the amount of Si in the electrode. This is also reflected in the respective charge capability tests, where electrodes with smaller Si content showed better power performance. With the aim to improve the charge capability of the electrode formulations, two approaches were evaluated: 1) addition of various amounts of conductive additive in the form of carbon black and 2) densification of electrodes. While the charge capability could be successfully improved by increasing carbon black content, densification mainly lead to performance deterioration.

1. Introduction

Fast charging and high-energy batteries are two critical key performance indicators for the electrification of the transport sector.^[1,2] State-of-the-art lithium-ion batteries (LIBs) contain a graphite negative electrode and a transition-metal-oxide positive electrode. In general, fast charging of LIBs is considered limited by the passivation layer, the solid-electrolyte-interphase (SEI), formed on the graphite electrode,^[3,4] which represents an additional barrier for Li-ions to cross at the electrode-electrolyte interface. Recent studies suggest that so-called high-voltage cathode materials, such as spinel-type lithium nickel-manganese-oxides (LNMO), also contribute to larger cell resistances due to electrolyte oxidation at high potentials.^[5]

At first glance, fast charging and high energy are two properties that appear to be difficult to combine in a practical battery cell: high-energy electrodes are typically dense with low porosity and have comparatively high coating thickness. Both thickness and low porosity of electrodes hamper ionic transport in and out of the electrode and, thus, limit the fast-charge capability of higher-energy batteries.^[2,6] Fast-charging batteries are designed focusing on quite the opposite properties: a reduced electrode density (i.e., higher porosity), larger amounts of conductive additive (improved electronic conductivity) and thinner coatings (shorter diffusion pathways), promoting fast-ion transport at the expense of volumetric energy density. Similarly, electrode materials that operate within the stability window of the electrolyte, such as lithium titanate (LTO),^[4] can improve the reaction kinetics tremendously due to the absence of a 'classical' SEI layer. Unfortunately, this

reduces the cell voltage with respect to the positive electrode and, hence, the energy density. As a counteraction to a reduced voltage window in LTO cells, pairing with high-voltage cathodes is often considered. Although, so-called 5 V-materials can increase the cell voltage, it should be noted that this approach merely shifts the problem of resistive surface layers from the anode to the cathode, and requires different electrolyte solvents with improved anodic stability.^[7]

Hence, the question arises of how to combine the best of both worlds. Controlling the electrode structure is one approach, which has been shown to improve the rate capabilities of graphite electrodes, e.g. when platelet-shaped graphite particles are aligned perpendicularly, rather than horizontally or randomly, with respect to the current collector.^[8] Another option is to use a negative electrode with a larger specific charge than graphite. As a result, the electrode coating would be thinner in a battery, where energy and all other parameters remain the same. Alternatively, when using capacity-enhancing additives, the electrodes could have a higher porosity, but the same coating thickness, which would reduce ionic-transport limitations. The specific charge of a graphite electrode can be increased, for instance, by addition of small amounts, i.e. less than 20 wt.%, of silicon particles.

In our previous work we have demonstrated that the lifetime of such graphite-Si blends is strongly dependent on the Si content.^[9] It has also been established^[6] that the discharge (= delithiation) rate capability of graphite is better than the charge (= lithiation), and therefore, in this study we aim to clarify how the addition of Si to graphite-Si blends affects the overall rate performance. Because of the relevance of fast-charging for many electronic devices, and especially so for electrical vehicles, we have focused in this work specifically on the charging capabilities of graphite-Si electrodes. We aim to understand the impact of the addition of Si to cell resistance and to verify viability of electrode densification and enhanced

[a] Dr. F. Jeschull, Dr. S. Trabesinger
Battery Electrodes and Cells, Electrochemistry Laboratory, Forschungsstrasse
111, 5232 Villigen PSI, Switzerland
E-mail: sigita.trabesinger@psi.ch

 Supporting information for this article is available on the WWW under
<https://doi.org/10.1002/batt.202000177>

electronic conductivity as approaches to improve the charge capability.

Experimental Section

Electrode Preparation and Cell Assembly

Graphite and graphite-Si blends were prepared according to a previously reported procedure.^[9,10] Briefly, a mixture of CMC–Na (Alfa Aesar) and PAA (25 wt.% aqueous solution, Sigma Aldrich) were added to a water:ethanol mixture (v/v = 70:30) and carbon black (CB, SuperC45, Imerys Graphite & Carbon), Si nanoparticles (30–50 nm average particle size, 70–80 m² g⁻¹ surface area, Nanostructured & Amorphous Materials Inc.) and graphite (KS6L, Imerys Graphite & Carbon) were blended into the slurry one after another, using a stirrer (IKA Ultra Torrax T25) at 16000 rpm by stirring for 2 minutes after each addition. The exact electrode compositions are given in Table 1. The slurries were coated on copper foil (20 µm, Schlenk Metalfolien) and dried first at ambient conditions and then for 2 hours at 150 °C under vacuum. Calendered samples were densified on a laboratory calender (Siemens) with a roll-pressure of 4 bars at a roll temperature of 40 °C. The calendering gap was reduced gradually in 3 steps to reach a maximum densification under the given conditions. Both, the as coated and the calendered electrodes were cut in discs of 13 mm in diameter and dried in the antechamber of an Ar-filled glovebox overnight at 120 °C under reduced pressure. The dried electrodes were assembled in coin-cell-type half-cells with Li as counter and reference electrode (750 µm thickness, purity 99.9%, Alfa Aesar). Prior to use, glass-fiber separators (EJJ 116, Hollingsworth & Vose, UK) were dried at 150 °C under vacuum. The separator was soaked with 500 µL of

electrolyte – a mixture comprising LP30 (1 M LiPF₆ in EC:DMC, v/v = 1:1, BASF) and 4 wt.% FEC (BASF).

Electrochemical Testing

Galvanostatic cycling and charge-capability tests were carried out on an Astrol battery cycler (Astrol Electronics AG, Switzerland). Intermittent current interruption experiments were conducted on a Biologic MPG-2. All cells were stored in a temperature chamber at 25 °C during the measurements.

Galvanostatic Cycling

Cells were cycled using a constant-current-constant-potential (CC-CP) cycling protocol. During the first cycle, the cell was cycled in the CC step with current of C/25, both for lithiation and delithiation (1 C equals the current corresponding to the specific charge of the respective electrode formulations, as given in Table 2). On following cycles, lithiation was carried out at C/10 and delithiation at C/3. The voltage cut-offs were placed at 5 mV and 1.5 V vs. Li⁺/Li. The current cut-off in the CP step was C/20 (C/50 for the first cycle). The data evaluation was performed with in-house developed analytical scripts based on the 'R' language (examples scripts are available, for instance in Ref. [11,12]).

Charge Capability Tests

Different charging rates were applied by altering the galvanostatic cycling schedule. The voltage cut-off limits of 5 mV and 1.5 V, as well as the discharge rate of C/3 remained the same in all cycles. As in the previous cycling schedule, the CC-step was followed by CP-step with a current cut-off of C/20 (except for the first cycle, as

Table 1. Electrode compositions.

Formulation	Graphite type	Graphite content [wt.%]	Silicon content ^[a] [wt.%]	Carbon black content ^[b] [wt.%]	Binder content ^[c] [wt.%]	Final solid fraction (slurry) ^[d] [%]
1	KS6L	95	0	1	4 (CMC:PAA)	31.4
2	KS6L	90	5	1	4 (CMC:PAA)	30.4
3	KS6L	85	10	1	4 (CMC:PAA)	31.3
4	KS6L	80	15	1	4 (CMC:PAA)	29.8
5	KS6L	75	20	1	4 (CMC:PAA)	29.1
6	KS6L	89.1	4.9	2	4 (CMC:PAA)	30.4
7	KS6L	87.2	4.8	4	4 (CMC:PAA)	29.9
8	KS6L	83.4	4.6	8	4 (CMC:PAA)	27.7

[a] Si nanoparticles, 30–50 nm. [b] Super C45. [c] 1:1 mixture of CMC–Na and PAA. [d] Solid fraction = active materials, carbon black & binders.

Table 2. Electrode properties from an average of at least 4 per formulation.

Formulation	Electrode loading [mg cm ⁻²]	Electrode thickness [µm]	Electrode density [mg mL ⁻¹]	Specific charge ^[a] [mAh g ⁻¹ AM]
1	4.94	107	0.58	372
2	6.22	130	0.63	541
3	5.27	113	0.60	709
4	5.87	121	0.62	878
5	5.47	122	0.60	1047
6	6.09	121	0.60	541
7	5.98	121	0.60	541
8	6.24	124	0.60	541
1-cal	7.07	77	1.24	372
2-cal	5.95	76	1.21	541
4-cal	5.69	82	1.02	1047

[a] The values refer to the sum of the specific charge per mass of the active materials, graphite and silicon.

described above). At the start, the cells were allowed to perform the conditioning cycle at C/25, and then three C/10-C/3 cycles, before the charging rate was altered for 5 consecutive cycles. Between sequences of altered charging rates, three C/10-C/3 cycles were carried out. The charging rates examined were 2 C, 1 C, C/2, C/4, C/8 and C/20 (according to the specific charge of each formulation, given in Table 2), summing up to a total of 49 cycles.

Intermittent Current Interruption (ICI) Measurements

Internal resistances were determined in a current-interruption experiments, performed on a Biologic MPG-2 multichannel potentiostat. 2-electrode cells were first cycled regularly for one cycle at C/25 (current cut-off in the CP-step was C/50) between 5 mV and 1.2 V, and the cell was then subjected to a cycle-relaxation (OCV) loop. A current of C/25 was applied for 30 min on the cell before it was allowed to relax again for 30 min. The potential relaxation was measured every 10 s or when a potential change was larger than 5 mV. If the potential at the end of the relaxation interval was larger than 45 mV vs. Li/Li⁺ upon lithiation and 0.9 V vs. Li/Li⁺ upon delithiation, respectively, the loop was repeated.

2. Results and Discussion

The electrodes used in this study comprise of a platelet-shaped graphite particles and Si nanoparticles. In the first part of this work the active material content in electrodes was fixed to 95 wt.%, of which 5–20 wt.% was Si, and some of the formulations were tested at two electrode densities. In the second part, the charge capability was tested by varying carbon black content in the electrodes, while the graphite-Si ratio remained constant.

2.1. Fast Charging Experiments

The charge capability tests of the graphite-Si half-cells was conducted with a constant-current-constant-potential (CC-CP) charging sequences, see experimental. The CC-charging step was performed at C-rates between 2 C and C/20, starting with the fastest rate of 2 C. While the CP-charging step guaranteed reaching the maximum achievable charge capacity. The discharge rate was held constant over all cycles at a rate of C/3. The cells were cycled at each charging rate for 5 cycles. In between different charging rates, a sequence of 3 cycles was introduced during which the CC-CP charging rate was reduced to C/10 in the CC-charging step. This sequence can be considered as a control experiment that shows if the cell was damaged by the applied charging current in the previous sequence, and how large the practically achievable specific charge of the electrode still is. In addition, the cell performed a formation sequence comprising one cycle at C/25 (charge and discharge) and three cycles at C/10 (charge) & C/3 (discharge).

This cycling procedure contrasts with commonly used procedures in literature, where the charge and discharge rates increase gradually by the same rate, resulting in ‘staircase-like’ rate-capability plots. In many cases purely galvanostatic cycling, without a CP-step, is applied. However, the CP-charging step is

of practical relevance, as it the most commonly used charging protocol of commercial LIBs.^[2,13] The CP-step not only improves the depth of charge but also reduces the internal resistances, such as the current decays, thus reducing overpotentials and mass-transport limitations that may induce Li plating towards the end of charge.^[2,13,14] It is important to note that there is no loss in information as the separation of the CC- and CP-contributions in the cycling data is straightforward using analytical scripts in common programming languages. Furthermore, it should be considered that the consequence of any incomplete galvanostatic charging (no CP) is a partial discharge and that the rate-capability of charge and discharge can be quite different, as reported by Buqa *et al.*^[6] In other words, in cycling protocols, in which charging is conducted without a CP-step, an evaluation of the discharge capabilities of an electrode is not definitely determinable, since the discharge is restricted by the charging performance to start with. The potential range might not be examined fully during such a discharge test, e.g. in electrode materials with step-like potential profiles such as graphite the plateau located at potentials closer to the Li-plating potential would not be accessed in such cycling schedules. Therefore, we exploit the combined CC- and CP-charging sequence to acquire a complete set of information.

2.2. Dependence on Si Content

The charging capability of graphite electrodes comprising 5 wt.%, 10 wt.%, 15 wt.% and 20 wt.% Si (uncalendered; electrode densities ca. 0.6 g mL⁻¹) are shown in Figure 1. The figure is divided in two panels showing the total charge capacity of the

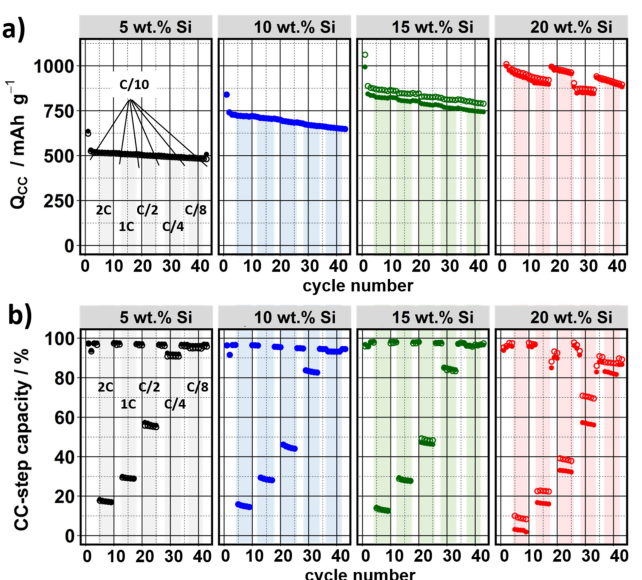


Figure 1. Charge capability test for graphite-Si electrodes with Si contents of 5 wt.%, 10 wt.%, 15 wt.% and 20 wt.% Si. The results of two cells per formulation are shown. a) total charge capacity (CC + CV step) and b) charge capacity transferred in the CC-step. The charging rate was varied in the rate-steps (indicated by the color bars) between 2 C and C/8. Between two rate steps three cycles with a charging rate of C/10 were carried out. The discharge rate was kept the same in all cycles.

cell per cycle (top panel), i.e. the sum of the CC- and CP-step contributions, and the fraction of charge, which was transferred in the CC-step (bottom panel). For each formulation, two cells are shown in the panels a-d, indicated by a full and empty symbols of the same color. A Si-free reference sample is provided in Figure S-1. In general, the CC-charging contribution should be as close to the specific charge of the electrode as possible. As the cell switches into the CP-charging the current decays exponentially and, therefore, the charging slows down as the charging time is not a linear function of the applied current anymore.^[2] If this point is reached very early into the charging process, the current does not decay exponentially, but a step-like decay is observed instead (Figure S-2). This behavior is in accordance with a previous study, where it was demonstrated that the deliberate use of solely the CP-charging (no CC sequence) affects the cycle life of batteries adversely.^[14]

As mentioned above, the cycling schedule starts with the fasted charging rate, 2 C, after the initial conditioning cycles. The charging rate is then reduced gradually to 1 C, C/2, C/4 and C/8 (so-called derating^[13]), including the aforementioned intermittent recovery & check-up cycles. As the charging rate decreases, the fraction of charge that is transferred in the CC-step increases notably. For a 2 C charge, the CC-contribution is below 20% for all Si-contents. Furthermore, it can be seen that the CC-contribution decreases as a function of increased Si content, with the electrode containing 20 wt.% Si showing the lowest CC-contribution below 10%. This formulation has also shown the least reproducibility between the measured specific capacity of the two cells, Figure 1a. As we have reported in our previous works, the electrode blends become increasingly inhomogeneous, as the Si content increases^[9,10] and, therefore, it is not surprising that larger variances in capacity are observed between samples of this formulation.

Only after the charging currents were decreased significantly to C/4 or below, more than 80% of the total capacity is transferred in the CC-step. A CC-contribution of more than 80%, i.e. a state-of-charge (SoC) of 80%, is a commonly used target for charging commercial batteries, before the charging protocol switches into the CP-step.^[2,13,15] In Figure 1b, the 5 wt. % Si formulation reaches under these conditions already CC-step contributions of more than 90% of the total charge capacity. Formulations with 10–15 wt.% Si charge up to about 80–85% under the same conditions. Again, the 20 wt.% graphite-Si composite shows the worst charge capability at C/4 and its CC-step contribution lies still below 80%. Besides the poorer charge capabilities with increasing Si content, a stronger capacity fading is observed in the order 5 wt.% < 10 wt.% < 15 wt.% < 20 wt.% of Si. The failure modes of these electrodes have been discussed in detail in previous works.^[9,10,16–19] Interestingly, a Si-free electrode formulation shows similar poor charge capability for 2 C (Figure S-1), but the charge capability improves in comparison to Si-containing formulations more rapidly with reduction of charge rates. At a charging rate of 1 C, more than 50% and at C/2 already more than 90% of the charge is transferred in the CC-step in Si-free graphite.

In contrast to the comparatively poor charge capabilities of the graphite-Si composites, it was observed that the discharge

rate can be as high as 2 C without any significant contributions from the CP-step for electrodes containing no or only 5 wt.% Si. At a Si content of 10 wt.%, the electrode was still able to provide more than 80% of the total capacity in the CC-step at 2 C, as shown in Figure S-3. As mentioned earlier, for graphite electrodes the bottleneck is mainly the charge capability,^[6] – same appears to apply to blends of graphite and Si.

Even for densified graphite electrodes, it has been shown that in coin-cells, the overpotential of the negative electrode increases considerably with increasing current density.^[20] And even the coin-cell material (stainless steel or aluminum) can have an impact on the resulting impedance, as demonstrated recently by Dahn and coworkers.^[21] Although the setups are not directly comparable, pouch cell stacks (full-cells) do not appear to suffer from equally strong overpotentials during fast charging.^[1] Unfortunately, performances of full-cells are seldom compared between different cell setups, and lab-scale experiments are mostly carried out in half-cells. Marinaro et al., for example, reported a capacity retention of over 90% for a graphite/Si-alloy blend at 1 C, while in corresponding half-cell experiments the capacity retention decreased much earlier.^[22] The difference between pouch and coin-cells (besides the counter-electrode) is a purely pressure-dependent ('point-to-point') contact between current collector and back contact, whereas the tabs of larger pouch-cell stacks are soldered. As a result, a limiting current density is reached in coin-cell-type setups faster.

On an electrode level, it is worth considering, that contact resistances may be caused by poor particle-particle contacts or a poor percolated conductive network. This problem is linked to the electrode preparation and can be dependent on the relative ratio between the electrode components. For example, depending on the CB-to-binder^[23] ratio and the choice of binder,^[20,24] insulating polymer layers may be formed on the particle surface of CB and active material, which affects the electronic and ionic transport properties^[25] of the electrode. If carbon black forms a percolated network or agglomerates is also influenced by the CB-to-binder ratio and has an impact on the electrode homogeneity.^[26] The particle orientation of the µm-sized graphite particles is also important as it can result in longer diffusion pathways for Li-ions and, thus, affect the mass-transport resistance in the porous electrode.^[8,27] Moreover, the contact resistance increases over time, as the SEI continues to grow on each cycle.^[5,28]

2.3. Current Interruption Experiments

Rate-limiting electrochemical reactions can be further identified more clearly by analysis of the internal resistance of the cell at different SoC, using a variant of the galvanostatic intermittent titration technique (GITT). GITT was originally developed to measure the solid-state diffusion of charge carriers in an electrochemically active material and uses constant-current pulses for a short time interval, followed by an open-circuit period, in which the cell potential is allowed to relax.^[29–31] In a more general scope, GITT is an intermittent current-interruption

(ICI) measurement^[5,12,32] that can be used to determine either the instant IR drop after the current has been turned off, or the difference between the reaction potential and OCV. The latter represents the sum of occurring resistances in the cell, i.e. the internal resistance. Although ICI experiments do not provide a similar level of detail as electrochemical impedance spectroscopy (EIS), they are less complex to analyze and offer a straightforward interpretation of the results, which in many cases is sufficient for the problem at hand.^[32]

Previous works proposed that an interruption can be as short as 0.5 s to determine the internal resistance.^[12,32] For the experiments herein, a comparatively long relaxation time of 30 min (OCV sequence) was chosen, in order to allow the system sufficient time for the potential relaxation. This way round, 100–120 interruptions per cycle were performed. The current rate under load (between current interruptions; CC-sequence) was C/20. From the data, the potentials at the end of the CC-sequence and at the end of the OCV-sequence were extracted and plotted against the SoC. The result is a plot that shows the difference between the electrochemical reaction potential at a given rate and the OCV potential of the electrode. For an easier comparison between electrodes with different specific charge, the potentials are plotted against state-of-charge (SoC) instead of capacity. Because in this study emphasis is placed specifically on the charging process, only the charging sequence is shown. In the example given in Figure S-4 for a graphite-Si blend, comprising 5 wt.% Si, it can be seen that the difference between the OCV and CC potentials for a particular interruption decreases with increasing degree of lithiation. This behavior can be attributed to the higher conductivity of Si-Li alloys, as well as to the Si-particle volume expansion during lithiation, which improves the particle-particle contacts in the electrode with increasing degree of lithiation. In addition, it should be noted that the first lithiation process to occur is the lithiation of amorphous Si, which is associated with a larger internal resistance, and therefore, the

resulting overpotential for the lithiation might hamper the charging of the electrode in the beginning.

In Figure 2, the internal resistance evolution during lithiation is compared between three electrode formulations comprising 0 wt.%, 5 wt.% and 20 wt.% Si. The gap between the OCV (full circles) and CC (empty circles) profiles is an indicator for the electrode resistance (assuming the resistances of other cell components are similar in all cases). In general, the gap is increasing from a Si-free graphite electrode, over a graphite electrode containing 5 wt.%, to a formulation with 20 wt.% Si. Moreover, a closer look at the profiles of the Si-containing electrodes shows that the gap changes for Si-containing graphite electrodes with the state of charge. In the potential region above 0.2 V vs Li⁺/Li, the first alloying reaction of Si from amorphous Si to Li_xSi-alloys is expected. In the lower potential regions, the lithiation of Si and graphite occur simultaneously and the potential gap narrows.

The trends become more obvious when the overpotentials are plotted against SoC, as shown in Figure 3. In particular, the potential differences at the beginning of the charging process display a notable increase with the higher amount of Si used in the electrode. A drop in overpotential, which is proportional to the length of the first Si alloying region, is noted after this initial lithiation step at a potential of around 200 mV vs. Li⁺/Li. Although the overpotential is generally decreasing after this first lithiation step, temporarily increasing overpotentials are found around the phase-transitions of graphite intercalation reactions (at the end of the plateau). In the phase-transition region, a potential hysteresis is observed, where the potential under load already reached the next plateau, but returns at OCV to potentials of the previous intercalation plateau, as can be seen by the lateral offset between the two profiles (OCV and end-of-charge phase) in Figure 2. The degrees of freedom at the end of a plateau are decreasing rapidly, as the last empty sites within the graphene sheets are occupied by Li to reach a stoichiometric composition. Under the conditions of an applied

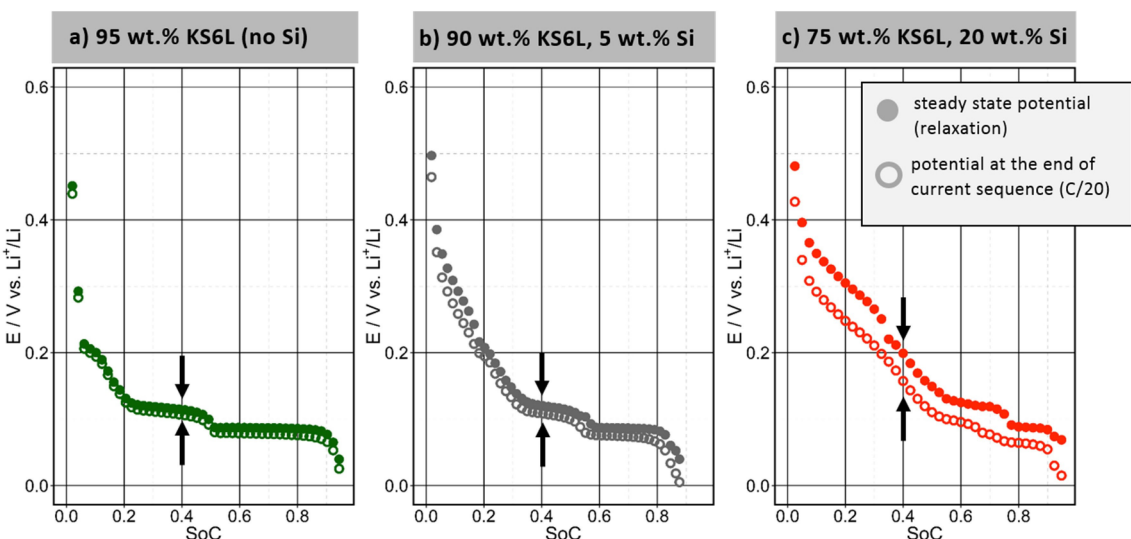


Figure 2. Current-interruption measurements during a slow charge at a rate of C/20 for three different electrode formulations with 0 wt.%, 5 wt.% and 20 wt.% Si.

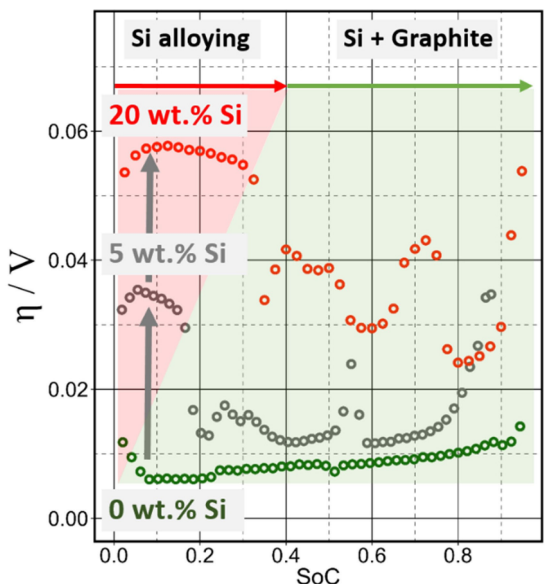


Figure 3. Differences in overpotentials as a function of SoC between graphite-Si electrodes with 0 wt.%, 5 wt.% and 20 wt.% of Si.

current (non-equilibrium conditions), the reaction enthalpy might favor the next lower intercalation plateau over the filling the last empty sites of the previous stage fully. Surprisingly, it is the Si-free graphite electrode that is least affected by this hysteresis effect and, instead, exhibits a quasi-linear increase in the potential gap with SoC. The overpotentials in Si-containing electrodes appear to be affected much stronger by the staging behavior of graphite, and appears to become more pronounced with increasing Si-content. One explanation could be an exchange of charge carriers during the OCV sequence in this phase-transition regions between Si and graphite, to balance the chemical potentials of the two active materials. During the phase-transition, this balance could be disturbed by the sudden potential drop to the next intercalation stage. Such a ‘charge-transfer interaction’ was also postulated by Dose *et al.*^[17] Possible mechanisms have so far not been proposed due to the lack of hard experimental evidence for such a process.

Towards the end of lithiation, a steep resistance increase is observed in these formulations. It is possible that at this point the graphite lithiation is complete, while Si continues to take up more lithium. At high degrees of lithiation, Si–Li alloys undergo another phase transition to form the metastable crystalline Li₁₅Si₄-alloy,^[33] which according to Key *et al.*^[34] can also be overlithiated to form a more reactive composition.

In summary, the experimental data suggests that the addition of Si to a graphite electrode is associated with an increasing overpotential in the beginning of the charging process. The charging capabilities of a graphite-Si electrode suffer from this shortcoming, since in this region, Si is the only reacting active material, having slower reaction kinetics than graphite. However, poorer particle connectivity at the onset of charging due to the significant volume changes of the Si-nanoparticles presumably play a decisive role as well. Furthermore, amorphous, delithiated Si particles are considered poor

electronic conductors, thus compromising a percolated conductive particle network.^[35] It is also known, that the volume expansion and contraction of Si particles causes recurring SEI layer formation, – thus a comparatively thick layer is formed, which impedes reactions at the electrode-electrolyte interface.^[36]

In the following sections, two common approaches are examined in attempt to improve the poor charge-capability and to reduce high overpotentials in the electrode coating by increasing 1) the coating density to improve particle contact and 2) the amount of conductive additive to improve electronically conductive network.

2.4. Electrode Density

The graphite electrodes, containing no (0 wt.%) and 5 wt.% of Si, were calendered to a coating density of around 1.2–1.3 g mL⁻¹ (porosities between 42–47%). Electrodes containing 20 wt.% only reached densities of around 1.0–1.1 g mL⁻¹ under the same calendering settings. The lower density with higher amount of Si can be attributed to the larger amount of nanoparticles in the electrodes, which occupy a significant volume fraction of the electrode at such high Si-contents. Increasing the roll pressure to up to 7 bar or using smaller slit widths did not affect the density, thus reaching the densification limits of the used equipment. For high-power application, lower electrode densities are more acceptable than for high energy-density applications, where electrode densities are ranging rather between 1.5–1.8 g mL⁻¹ (= porosities between 20–30%).^[37] In our experiments we were not able to reach electrode density fit for high-energy density cells.

The charge capability test, as shown above, was repeated on the densified electrodes (Figure 4). Contrary to expectations,

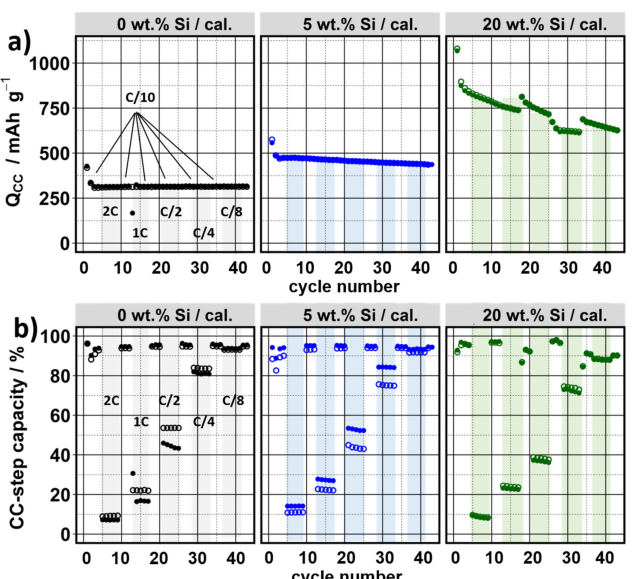


Figure 4. Charge-capability test of calendered graphite-Si electrodes, containing 0 wt.% (a), 5 wt.% (b) and 20 wt.% Si (c). The results of two cells per formulation are shown.

the charge-capability is adversely affected by the densification, which applies to both Si-containing formulations, as well as the Si-free electrode. Moreover, it can be seen that the capacity retention is poorer for calendered Si-containing electrodes than for uncalendered ones. The Si-free sample shows a comparatively stable cycling behavior after a drop during the few initial cycles. It reaches 80% SoC in the CC-step at charging rates $\leq C/4$. A rather similar behavior is observed for the 5 wt.% Si sample, which shows only a slight capacity fade over the 45 cycles. At the fastest rates, i.e. 1 C and 2 C, the 5 wt.% Si formulation appears to perform slightly better than the Si-free electrode composition, even though this difference might be considered negligible, given the overall poor charging capabilities at these rates. As in Figure 1, the electrode comprising 20 wt.% Si suffers from a strong capacity fade in combination with a poor charge capability. At a charging rate of C/4, the electrodes take up still less than 80% of their total capacity during the CC-step. The effect can likely be attributed to the large expansion coefficient of the Si-nanoparticles. Previous reports on densified Si electrodes (without graphite) have shown that the capacity fade increases with electrode density.^[38,39] Taking into account these findings, it is thus reasonable to assume that graphite-Si electrodes with larger Si contents would suffer from stronger capacity fading, as seen in our experiments.

As mentioned previously, at high-rate cycling might be associated with setup-related limitations. Although densification of the electrodes may improve the electronic conductivity of the percolated conductive network, this will not remove the contact issues between the cells back and current collector. The fact that the Si-free electrode also exhibits a poor charge capability suggests that some of the problems are rooted in the electrode formulation and, in particular, in the graphite used in this study. The choice of the graphite was based on previous findings, which suggested that smaller graphite particles show a better capacity retention and – at least for small Si contents – a more uniform material distribution.^[9] In theory, one would expect smaller graphite particles to show better rate performance as well, as more diffusion pathways are available for the electrolyte to supply the active materials with Li-ions.^[6] According to Cericola *et al.*, the electrode porosity, formed by a particular graphite in an electrode coating, can be correlated to its particle size and shape, and can thus vary greatly depending on the material chosen.^[40] In addition, more interparticle contacts allow for a more uniform charge distribution.^[6] However, electrode porosity and diffusion pathways are only part of the picture. A high porosity is not necessarily beneficial, if the pores are small and/or the porous network is highly branched, as such pore networks will affect the pore resistance and, hence, the mass transport.^[41,42] In other words high tortuosity can impede fast charging.^[43] From this point of view, the orientation and distribution of active material particles can play an important role, as previously demonstrated by Billaud *et al.*^[8] and Müller *et al.*^[44] In the former study, the reference sample with predominantly horizontally aligned particles (with respect to the current collector surface) showed similarly poor rate-capability properties as in the cases

presented in Figure 1 & 3. Vertically aligned particles, on the other hand, showed improved rate performance at high rates. As demonstrated in our previous study,^[9,10] the graphite particle-alignment is predominantly horizontal with respect to the current collector for the electrodes used herein, giving explanation to the poor performance observed.

2.5. Conductive Additive Content

Lastly, the effect of different conductive additive contents was studied for the graphite-Si electrode with 5 wt.% Si. So far, for all experiments the carbon black (CB) content was limited to 1 wt.%. In Figure 5, the performance of electrodes, where CB content was raised to 2, 4 and 8 wt.%, is shown. A study on calendered electrodes was not considered herein, since our previous results (comparison Figure 1 & 3 and Ref. [10]) have shown that the densification is detrimental to the capacity retention and has no positive impact on the charge capability. With respect to capacity retention, the electrodes perform all similarly to the CB of 1 wt.% reference sample. The differences in the charge-capability can be seen to take a notable effect only when CB content is raised to 4 wt.% and 8 wt.%. The 80% SoC in the CC-step is approached already at C/2 with 4 wt.% CB, i.e. electrodes tolerate twice the current-density as compared to 1 wt.% of CB, and even higher with 8 wt.% CB. Faster rates are affected positively as well: at 1 C the CC-step contribution increases from 30% to 40%. The effects responsible for these improvements are associated with various effects: an increase in the CB-to-binder ratio may affect the binder distribution,^[11,45] the electronic conductivity^[46,47] as well as the pore tortuosity and percolation of the CB-binder mixture within the electrode.^[42,48,49] In fact, small changes in the CB-to-binder ratio can trigger formation of inherently different

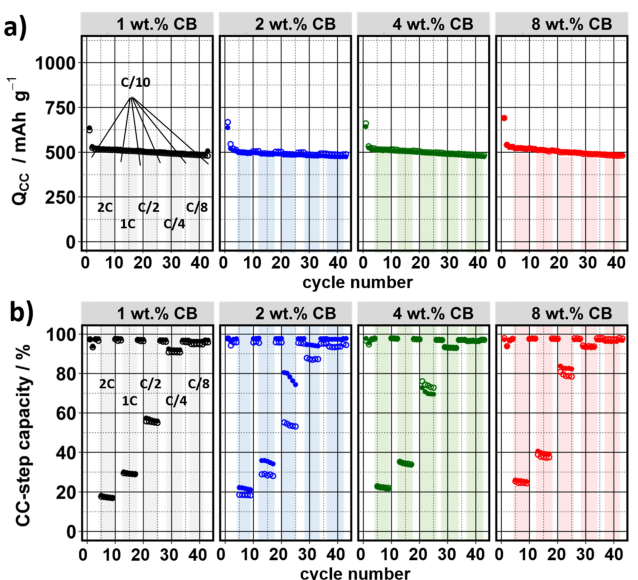


Figure 5. Charge capability test for graphite-Si electrodes with 1 wt.% CB (a), 2 wt.% CB (b), 4 wt.% CB (c) and 8 wt.% Si (d). Shown are the results of two cells per formulation.

particle networks that strongly affect the electronic conductivity and interfacial impedance. Besides, a series of studies by Battaglia and coworkers^[23,26,50] on the CB distribution and electronic conductivity in NCA:PVdF composite electrodes, this is rarely investigated and is a frequently overlooked property, which often surfaces indirectly in qualitative observations, such as agglomerated CB domains within the electrode.^[39,51] In an electrode slurry, binders also act as surfactants^[25,52,53] that cover the surface of the individual electrode components, whose specific surface area thus determines, how much binder deposits on each interface at a fixed binder content.^[20] Because of the significantly higher surface area of CB, the majority of the binder fraction typically ends up on CB, causing the conductive additive to agglomerate. Such agglomerates can be tolerated as long as a percolated conductive network is sustained. As demonstrated by Bauer *et al.*, the opposite case, i.e. an uniform coverage of active material particles by CB, is not necessarily a favorable situation either, if the electrode is lacking a percolated CB network.^[25] In addition, excess binder can result in the formation of polymer layers on the active material surface, resulting in higher interfacial impedance.^[25,26,45] On the other hand, it is worth mentioning that polymeric layers of binders that dissolve poorly (or not at all) in the electrolyte also have a protective effect.^[24,54–57] Therefore, Liu *et al.*^[26] concluded that the CB-to-binder ratio can be used to tailor the properties of the electrode between high-power and high-energy applications.

Previous studies on CB:PVdF mixtures suggest that the optimum amounts favor a slight excess of PVdF.^[23,26] However, the optimum ratio for CMC–Na, PAA or a combination of both has not been investigated as yet. The charge capability tests in Figure 3 show that the CC-step contribution increases with increased CB content, and therefore, it appears that the CB content has to exceed the amount of the CMC–Na:PAA mixture. Not all above-mentioned considerations hold for our system, because the surface areas of the Si and CB particles lie in a similar range, and are notably higher than the microsized graphite or NCA particles, used in aforementioned studies.^[23,26,50]

In summary, the simple assumption that CB generally improves rate capability is only partly accurate, as the relative amounts between CB and binder (as well as the type of binder) could have a profound impact on the electronic conductivity of the electrode.

3. Conclusions

In this work we have studied the charging behavior of graphite-Si blends at different charging rates. It has been shown that the charge capability decreases gradually with increasing Si-content in the electrode. An intermittent current-interruption method demonstrated further that the internal resistance, i.e. the potential differences between OCV and the reaction potentials, increase notably with increasing Si content. The additional resistance induced by the Si fraction in the active material blend can impede fast charging. Two strategies

have been tested to mitigate the poor charging behavior at high rates: 1) the densification of the electrode coating and 2) higher contents of conductive additive.

It was found that even at medium electrode densities (1.2–1.3 g mL⁻¹), Si-containing electrodes suffer from faster capacity fade when the electrode density is increased. Although the losses associated to denser electrodes are significantly reduced in comparison to (graphite-free) Si electrodes, the capacity fade is present in graphite-Si electrodes and is also dependent on the Si-content. In terms of charge capability, little improvement was observed with respect to uncalendered samples. The alternative approach, seeking to achieve faster charge rates by raising the carbon black content, improved the charge capability of electrodes comprising 5 wt.% Si at high rates (1 C and 2 C) only slightly, while considerably at intermediate rates (C/2–C/4). The electronic network in electrodes comprising only 1 wt.% CB can thus be further improved by increasing the amount of conductive additive, though at the expense of the active material loading.

This study has shown that additional cell resistances, related to poor charging capabilities, do not solely originate from the presence of Si, because even the Si-free graphite electrodes are lacking behind in cycling at the technologically-feasible rates as well, despite the small potential gaps measured during the current-interruption experiments. It is therefore likely that besides limitations of the active materials and the electrode architecture, intrinsic limitations of our cell setup are approached at high rates. Nonetheless, the experiments allowed a comprehensive comparison of fast charging limitations in graphite-Si electrodes and an evaluation of the effects of two common approaches to mitigate poor charge capability.

Conflict of Interest

The authors declare no conflict of interest.

Keywords: fast-charging • graphite-Si blends • intermittent current interruption • rate capability • lithium-ion batteries

- [1] Z. Du, D. L. Wood III, I. Belharouak, *Electrochim. Commun.* **2019**, *103*, 109–113.
- [2] A. Tomaszewska, Z. Chu, X. Feng, S. O’Kane, X. Liu, J. Chen, C. Ji, E. Endler, R. Li, L. Liu, Y. Li, S. Zheng, S. Vetterlein, M. Gao, J. Du, M. Parkes, M. Ouyang, M. Marinescu, G. Offer, B. Wu, *eTransportation* **2019**, *1*, 100011.
- [3] E. Pohjalainen, S. Räsänen, M. Jokinen, K. Yliniemi, D. A. Worsley, J. Kuusivaara, J. Juurikivi, R. Ekqvist, T. Kallio, M. Karppinen, *J. Power Sources* **2013**, *226*, 134–139.
- [4] B. Lee, E. Oh, *J. Phys. Chem. C* **2013**, *117*, 4404–4409.
- [5] B. Aktekin, M. J. Lacey, T. Nordh, R. Younesi, C. Tengstedt, W. Zipprich, D. Brandell, K. Edström, *J. Phys. Chem. C* **2018**, *122*, 11234–11248.
- [6] H. Buqa, D. Goers, M. Holzapfel, M. E. Spahr, P. Novák, *J. Electrochem. Soc.* **2005**, *152*, A474–A481.
- [7] M. M. Doeff, *Batter. Sustain. Sel. Entries from Encycl. Sustain. Sci. Technol.* (Ed.: R. J. Brodd), Springer Science + Business Media, New York **2013**, pp. 5–49.
- [8] J. Billaud, F. Bouville, T. Magrini, C. Villevieille, A. R. Studart, *Nat. Energy* **2016**, *1*, 1–6.

- [9] F. Jeschull, Y. Surace, S. Zürcher, M. E. Spahr, P. Novák, S. Trabesinger, *Electrochim. Acta* **2019**, *320*, 134602.
- [10] F. Jeschull, Y. Surace, S. Zürcher, G. Lari, M. E. Spahr, P. Novák, S. Trabesinger, *J. Electrochem. Soc.* **2020**, *167*, 100535.
- [11] F. Jeschull, F. Lindgren, M. J. Lacey, F. Björefors, K. Edström, D. Brandell, *J. Power Sources* **2016**, *325*, 513–524.
- [12] M. J. Lacey, K. Edström, D. Brandell, *Chem. Commun.* **2015**, *51*, 16502–16505.
- [13] T. Amietszajew, E. McTurk, J. Fleming, R. Bhagat, *Electrochim. Acta* **2018**, *263*, 346–352.
- [14] P. H. L. Notten, J. H. G. O. H. Veld, J. R. G. Van Beek, *J. Power Sources* **2005**, *145*, 89–94.
- [15] S. Ahmed, I. Bloom, A. N. Jansen, T. Tanim, E. J. Dufek, A. Pesaran, A. Burnham, R. B. Carlson, F. Dias, K. Hardy, M. Keyser, C. Kreuzer, A. Markel, A. Meintz, C. Michelbacher, M. Mohanpurkar, P. A. Nelson, D. C. Robertson, D. Scoffield, M. Shirk, T. Stephens, R. Vijayagopal, J. Zhang, *J. Power Sources* **2017**, *367*, 250–262.
- [16] M. Wetjen, D. Pritzl, R. Jung, S. Solchenbach, R. Ghadimi, H. A. Gasteiger, *J. Electrochem. Soc.* **2017**, *164*, A2840–A2852.
- [17] W. M. Dose, M. J. Piernas-Muñoz, V. A. Maroni, S. E. Trask, I. Bloom, C. S. Johnson, *Chem. Commun.* **2018**, *54*, 3586–3589.
- [18] W. M. Dose, V. A. Maroni, M. J. Piernas-Muñoz, S. E. Trask, I. Bloom, C. S. Johnson, *J. Electrochem. Soc.* **2018**, *165*, A2389–A2396.
- [19] K. Kalaga, M. T. F. Rodrigues, S. E. Trask, I. A. Shkrob, D. P. Abraham, *Electrochim. Acta* **2018**, *280*, 221–228.
- [20] F. Jeschull, D. Brandell, M. Wohlfahrt-Mehrens, M. Memm, *Energy Technol.* **2017**, *5*, 2108–2118.
- [21] A. S. Keefe, S. Buteau, I. G. Hill, J. R. Dahn, *J. Electrochem. Soc.* **2019**, *166*, A3272–A3279.
- [22] M. Marinaro, D. Yoon, G. Gabrielli, P. Stegmaier, E. Figgemeier, P. C. Spurk, D. Nelis, G. Schmidt, J. Chauveau, P. Axmann, M. Wohlfahrt-Mehrens, *J. Power Sources* **2017**, *357*, 188–197.
- [23] H. Zheng, R. Yang, G. Liu, X. Song, V. S. Battaglia, *J. Phys. Chem. C* **2012**, *116*, 4875–4882.
- [24] F. Jeschull, M. J. Lacey, D. Brandell, *Electrochim. Acta* **2015**, *175*, 141–150.
- [25] W. Bauer, D. Nötzel, V. Wenzel, H. Nirschl, *J. Power Sources* **2015**, *288*, 359–367.
- [26] G. Liu, H. Zheng, X. Song, V. S. Battaglia, *J. Electrochem. Soc.* **2012**, *159*, A214–A221.
- [27] F. Y. Su, Y. B. He, B. Li, X. C. Chen, C. H. You, W. Wei, W. Lv, Q. H. Yang, F. Kang, *Nano Energy* **2012**, *1*, 429–439.
- [28] D. Pitzl, J. Landesfeind, S. Solchenbach, H. A. Gasteiger, *J. Electrochem. Soc.* **2018**, *165*, A2145–A2153.
- [29] W. Weppner, R. A. Huggins, *J. Electrochem. Soc.* **1977**, *124*, 1569–1578.
- [30] N. Garcia-Araez, J. W. Dibden, N. Meddings, J. Owen, *ChemElectroChem* **2017**, *1*, 1–11.
- [31] T. Sasaki, Y. Ukyo, P. Novák, *Nat. Mater.* **2013**, *12*, 569–575.
- [32] M. J. Lacey, *ChemElectroChem* **2017**, *4*, 1997–2004.
- [33] S. Misra, N. Liu, J. Nelson, S. S. Hong, Y. Cui, M. F. Toney, *ACS Nano* **2012**, *6*, 5465–5473.
- [34] B. Key, R. Bhattacharyya, M. Morcrette, V. Sezne, J. Tarascon, C. P. Grey, *J. Am. Chem. Soc.* **2009**, *131*, 9239–9249.
- [35] T. Schott, R. Robert, P. A. Ulmann, P. Lanz, S. Zürcher, M. E. Spahr, P. Novák, S. Trabesinger, *J. Phys. Chem. C* **2017**, *121*, 18423–18429.
- [36] C. Xu, F. Lindgren, B. Philippe, M. Gorgoi, F. Björefors, K. Edström, T. Gustafsson, *Chem. Mater.* **2015**, *27*, 2591–2599.
- [37] E. J. Berg, C. Villevieille, D. Streich, S. Trabesinger, P. Novák, *J. Electrochem. Soc.* **2015**, *162*, A2468–A2475.
- [38] Z. Karkar, T. Jaouhari, A. Tranchot, D. Mazouzi, D. Guyomard, B. Lestriez, L. Roué, *J. Power Sources* **2017**, *371*, 136–147.
- [39] B. P. N. Nguyen, S. Chazelle, M. Cerbelaud, W. Porcher, B. Lestriez, *J. Power Sources* **2014**, *262*, 112–122.
- [40] D. Cericola, M. E. Spahr, *Electrochim. Acta* **2016**, *191*, 558–566.
- [41] S. Malifarge, B. Delobel, C. Delacourt, *J. Electrochem. Soc.* **2017**, *164*, E3329–E3334.
- [42] N. Besnard, A. Etiemble, T. Douillard, O. Dubrunfaut, P. Tran-Van, L. Gautier, S. Franger, J. C. Badot, E. Maire, B. Lestriez, *Adv. Energy Mater.* **2017**, *7*, 1–16.
- [43] M. Ebner, D. W. Chung, R. E. García, V. Wood, *Adv. Energy Mater.* **2014**, *4*, 1–6.
- [44] S. Müller, J. Eller, M. Ebner, C. Burns, J. R. Dahn, V. Wood, *J. Electrochem. Soc.* **2018**, *165*, A339–A344.
- [45] T. Marks, S. Trussler, A. J. Smith, D. Xiong, J. R. Dahn, *J. Electrochem. Soc.* **2011**, *158*, A51.
- [46] G. Liu, H. Zheng, S. Kim, Y. Deng, A. M. Minor, X. Song, V. S. Battaglia, *J. Electrochem. Soc.* **2008**, *155*, A887.
- [47] G. Liu, H. Zheng, A. S. Simens, A. M. Minor, X. Song, V. S. Battaglia, *J. Electrochem. Soc.* **2007**, *154*, A1129–A1134.
- [48] E. Panabière, J.-C. Badot, O. Dubrunfaut, A. Etiemble, B. Lestriez, *J. Phys. Chem. C* **2017**, *121*, 8364–8377.
- [49] L. Pfaffmann, S. Jaïser, M. Müller, P. Scharfer, W. Schabel, W. Bauer, F. Scheiba, H. Ehrenberg, *J. Power Sources* **2017**, *363*, 460–469.
- [50] G. Liu, H. Zheng, A. S. Simens, A. M. Minor, X. Song, V. S. Battaglia, *J. Electrochem. Soc.* **2007**, *154*, A1129.
- [51] T. Nordh, F. Jeschull, R. Younesi, T. Koçak, C. Tengstedt, K. Edström, D. Brandell, *ChemElectroChem* **2017**, *4*, 2683–2692.
- [52] J.-H. Lee, U. Paik, V. A. Hackley, Y.-M. Choi, *J. Power Sources* **2006**, *161*, 612–616.
- [53] J.-H. Lee, S. Lee, U. Paik, Y.-M. Choi, *J. Power Sources* **2005**, *147*, 249–255.
- [54] F. Jeschull, D. Brandell, K. Edström, M. J. Lacey, *Chem. Commun.* **2015**, *51*, 17100–17103.
- [55] S. Komaba, N. Yabuuchi, T. Ozeki, K. Okushi, H. Yui, K. Konno, Y. Katayama, T. Miura, *J. Power Sources* **2010**, *195*, 6069–6074.
- [56] S. Komaba, K. Okushi, T. Ozeki, H. Yui, Y. Katayama, T. Miura, T. Saito, H. Grout, *Electrochem. Solid-State Lett.* **2009**, *12*, A107.
- [57] A. Magasinski, B. Zdyrko, I. Kovalenko, B. Hertzberg, R. Burtovy, C. F. Huebner, T. F. Fuller, I. Luzinov, G. Yushin, *ACS Appl. Mater. Interfaces* **2010**, *2*, 3004–3010.

Manuscript received: July 22, 2020

Revised manuscript received: August 14, 2020

Accepted manuscript online: August 17, 2020

Version of record online: September 10, 2020